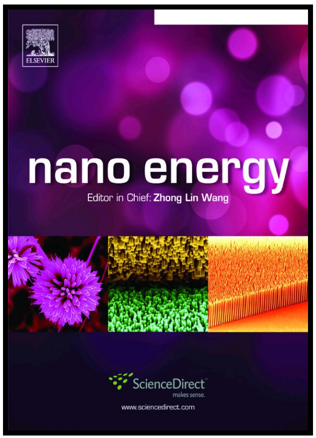
www.elsevier.com/locate/nanoenergy

Two-dimensional silicon suboxides nanostructures with Si nanodomains confined in amorphous SiO_2 derived from siloxene as high performance anode for Li-ion batteries

Rusheng Fu, Keli Zhang, Remo Proietti Zaccaria, Heran Huang, Yonggao Xia, Zhaoping Liu

PII: S2211-2855(17)30453-6
DOI: http://dx.doi.org/10.1016/j.nanoen.2017.07.040
Reference: NANOEN2098

To appear in: *Nano Energy*

Received date: 6 May 2017
Revised date: 11 June 2017
Accepted date: 24 July 2017

Cite this article as: Rusheng Fu, Keli Zhang, Remo Proietti Zaccaria, Hera Huang, Yonggao Xia and Zhaoping Liu, Two-dimensional silicon suboxide nanostructures with Si nanodomains confined in amorphous SiO_2 derived fror siloxene as high performance anode for Li-ion batteries, *Nano Energy* http://dx.doi.org/10.1016/j.nanoen.2017.07.040

Two-dimensional silicon suboxides nanostructures with Si nanodomains confined in amorphous SiO_2 derived from siloxene as high performance anode for Li-ion batteries

Rusheng Fu[a,c], Keli Zhang[a], Remo Proietti Zaccaria[b,d], Heran Huang[a], Yonggao Xia[a,]* and Zhaoping Liu[a,]*

[a] Advanced Li-ion Battery Engineering Laboratory and Key Laboratory of Graphene Technologies and Applications of Zhejiang Province, Ningbo Institute of Materials Technology and Engineering, Chinese Academy of Sciences, Zhejiang 315201, P. R. China

[b]Cixi Institute of Biomedical Engineering, Ningbo Institute of Materials Technology and Engineering, Chinese Academy of Sciences, Zhejiang 315201, P. R. China

[c] University of Chinese Academy of Sciences, Beijing 100049, P. R. China

[d] Italian Institute of Technology, via Morego 30, 16163 Genoa, Italy

Y. Xia (xiayg@nimte.ac.cn)

Z. Liu (liuzp@nimte.ac.cn)

*Corresponding authors:

Abstract

SiO_x owing to high reversible capacity and moderate volume expansion has been attracting a lot of attention as state-of-the-art anodes for the next generation of Li-ion batteries. However, poor cycling performance and poor rate capability, respectively associated with detrimental volume expansion and insulative amorphous SiO_2, are still challenging issues which need to be addressed for the actual employment as anodes for Li-ion batteries. In this regard, here we design, synthesize, characterize and test carbon coated sheet-like $SiO_{1.1}$ nanocomposites formed by Si-nanodomains confined inside amorphous SiO_2 (nano-Si/*a*-SiO_2). As a proof-of-concept, we achieve sheet-like SiO_x nanocomposites via in-situ transformation of delaminated siloxene. In particular, self-prepared siloxene with oxygen-inserted Si_6 rings terminated with H and OH ligands is prepared by delamination of $CaSi_2$ in dilute HCl. Importantly, the resulting carbon coated nano-Si/*a*-SiO_2 material shows enhanced reaction kinetics and structural stability leading to 946 mAh g^{-1} capacity at 0.15 A g^{-1}. Intriguingly, 38.0% (~360 mAh g^{-1}) of the maximum capacity is maintained even at 7.5 A g^{-1}, corresponding to a remarkable less than 3 minutes charge/discharge time. Finally, the electrode shows merely 24% of volume expansion and minor cracks with capacity retention of 92% after 300 cycles at 7.5 A g^{-1}.

Graphic Abstract

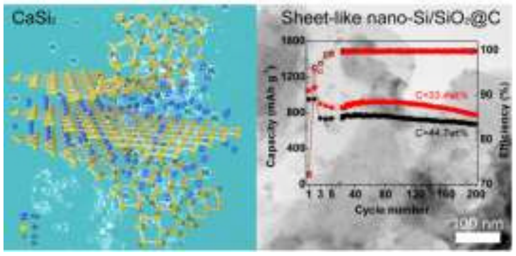

We introduce a strategy to prepare sheet-like Si/SiO_2 nanocomposites from siloxene. Siloxene was delaminated from layered $CaSi_2$. After CVD process, sheet-like Si/SiO_2@C showing Si nanodomains well confined within amorphous SiO_2 matrix exhibits superior electrochemical performance as anode for Li-ion batteries.

KEYWORDS: two dimensional nanostructures, siloxene, silicon suboxides, Si nanodomains, lithium ion battery

Introduction

Silicon-based materials are considered among the best anode candidates for the next-generation of Li-ion batteries due to the Si impressive theoretical capacity (3579 mAh g^{-1} for $Li_{15}Si_4$)[1-3]. However, the drastic volume change of Si (~300%) upon lithiation and delithiation gives rise to the loss of electrical contact and to excessive solid-electrolyte interphase (SEI) growth, which results in poor rate capability and cycling stability[4, 5]. Lately, two dimensional silicon so-called silicene attracted much attention which shows prospect for lithium-ion batteries[6, 7]. However, buckled honeycomb silicene, even multilayer silicene is not stable in air within 24 h[8]. Alternatively, nonstoichiometric silicon oxides such as annealed SiO that is formed by a matrix nanocrystalline Si dispersed in amorphous SiO_x (nano-Si/*a*-SiO_x), have also been exploited to effectively decrease the volume variation[9,10]. The presence of oxygen atoms in the mixture limits indeed the volume expansion, owing to the formation of irreversible by-products such as Li_2O and lithium silicate which play the role of buffer area. However, few approaches have been used to synthesize nonstoichiometric silicon oxides: (1) evaporation and condensation of Si/SiO_2 mixture at T >5000 ºC[11]; (2) carbothermic reduction of SiO_2 at T ≥1000 ºC with H_2[12]; (3) induction melting Si with the injection of various mixed gases[13]; (4) hydrogen silsesquioxane ($HSiO_{1.5}$) used to prepare Si/SiO_x nanospheres[14]. All the resulting samples show three dimensional structures that SiO_x was dispersed along with Si, where Li-ions need to migrate through lithium silicate or Li_2O layer after the first cycle, hence leading to poor rate performance. With this in hand and with the desire to overcome these drawbacks, we have aimed to the realization of two-dimensional silicon suboxides nanocomposites (2D-SiO_x) which show moderate volume variation and provide better electrons and Li-ions kinetics.

Herein, we introduce an innovative design of sheet-like Si/SiO_2 nanocomposites showing Si nanodomains well confined within the amorphous SiO_2 matrix (in brief nano-Si/*a*-SiO_2). These novel composites are received by annealing siloxene precursor which is obtained by topotactic transformation of layered $CaSi_2$[15, 16]. This unique material design brings about multiple merits with respect to electrochemical performance. Primarily, lithiation of *a*-SiO_2 matrix results in the formation of reversible Li-Si alloy together with irreversible lithium silicate and Li_2O, the latter known to act as buffering phases against volume expansion during cycling[17]. Furthermore, *in-situ* prepared Si nanodomains with size less than 10 nm are homogeneously dispersed and effectively alleviate the volume expansion stress. Foremost, the introduced unique sheet-like structure allows for faster Li-ion and electron diffusion which, in turn, mean superior electrochemical performance, especially a better cycling stability and improved rate properties.

Experimental section

Materials preparation.

$CaSi_2$ raw material (Sinopharm Chemical Reagent Beijing Co., Ltd) was initially purified by reaction with NaOH aqueous solution to remove any residual crystalline silicon. At air atmosphere, the as-received layered $CaSi_2$ was added in dilute HCl aqueous solutions (5 mol L^{-1}) with supersonic treatment for 15-20 h. Subsequently, black $CaSi_2$ was converted into insoluble greenish-yellow suspension here named as-prepared siloxene. Supersonic treatment (40 kHz) was used to facilitate the delaminating process. The as-prepared siloxene, after washing with deionized water, was dried by freeze drying. Subsequently, the as-received siloxene powders were subjected to anneal at 300, 400 and 900 ºC (with a heating rate of 10 ºC min^{-1}) for 3, 2 and 1 h under fixed flowing Ar atmosphere (≥99.999%) to obtain silicon suboxide (SiO_x) and nano-Si/*a*-SiO_2, respectively. Sheet-like nano-Si/*a*-SiO_2@C samples were finally synthesized under flowing Ar atmosphere for temperature below 900 ºC, followed by the flowing of C_2H_4 (100-200 sccm) when the temperature reached 900 ºC for 45 min.

Materials characterizations

The crystal structures were determined by X-ray diffraction (XRD, Bruker D8 Advance) with a Cu Kα radiation (λ = 1.5418 Å) operated at 40 kV and 40 mA. The morphologies and microstructures were examined using field emission scanning electron microscopy (FESEM, Hitachi S-4800) and transmission electron microscopy (TEM, Tecnai F20). Electron energy loss spectra (EELS) were recorded using a convergent-beam in STEM mode for imaging and spectroscopy. The optimal energy-resolution was ~0.35 eV, as judged by the full-with at half-maximum of the zero-less peak. Total acquisition time was 5 s for the Si $L_{2,3}$ edge. For SEM/TEM observations, the fully delithiated nano-Si/*a*-SiO_2@C was disassembled in Ar-filled glove box, rinsed with DMC and dried over night under vacuum. Raman spectra (Raman, Renishaw inVia Reflex) were collected from 200 to 1700 cm^{-1} with a He-Ne laser at the wavelength of 532 nm. The Fourier transformed infrared spectra (FTIR, Nicolet 6700) were collected from 400 to 4000 cm^{-1}. X-ray photoelectron spectroscopy (XPS, Axis Ultra DLD) measurements were performed using Al Kα monochromatic beam (1486.6 eV). All spectra are calibrated using C 1s peak (284.5 eV) from conductive tape. After the subtraction of the baseline (Shirley), the Si 2p curve fitting is performed using the non linear least-squares algorithm. Thermal gravimetric analysis (TGA, Perkin-Elmer Pyris Diamond) was used to evaluate the carbon content and O/Si atomic ratio. The ^{29}Si solid-state NMR experiment was performed on a Varian Infinity-Plus 300 NMR spectrometer. A double resonance 7.5 mm MAS probe was used at Larmor frequencies of 59.55 MHz for ^{29}Si. The ^{29}Si chemical shifts were determined by a solid external reference, Kaolin clay (-91.5 ppm). The sample was measured under a spin rate of 5 kHz.

Electrochemical measurements

The electrodes were prepared by casting slurries including the anode (75 wt%) as active materials, conducting agent (Super-P, 15 wt%) and binding agent (7 wt% of styrene butadiene rubber (SBR) and 3 wt% of carboxymethyl cellulose (CMC)) dissolved in deionized water on Cu foil. After casting, the electrodes were dried at 80 ºC for 8 h in air followed by 5 h in vacuum at 120 ºC, then pressed at 5 MPa. The areal mass loading is 0.8-1.2 and 0.6-0.8 mg cm^{-2} associated with nano-Si/*a*-SiO_2@C and siloxene electrode, respectively. The coin cells CR2032 were assembled using Li foil as a counter electrode within Ar-filled glove box (H_2O level <0.1 ppm and O_2 level <0.1 ppm). Celgard 2400 was used as separator, with 1 M $LiPF_6$ as commercial electrolyte in EC/DEC=1:1 by volume with 5 wt% FEC (Zhangjiagang Guotai-Huarong New Chemical Materials Co., Ltd.). The galvanostatic cycling was performed using Land CT 2100A battery-test system. The half-cells were discharged (Li^+ insertion) and charged (Li^+ extraction) in the potential range between 0.005 and 1.5 V under different current densities. The capacity was calculated on the basis of active materials. Cyclic voltammetry (CV) curves were recorded by Solartron using CR2032-type coin cells with scanning rate of 0.1 mV s^{-1} and voltage window at 0.005-2.0 V.

Results and discussion

Siloxene was synthesized by delaminating of commercial $CaSi_2$ as shown in Figure 1a,b. At first, the as-received $CaSi_2$ was rinsed with 5 mol L^{-1} NaOH aqueous solution to remove residual Si impurity, with exception of $FeSi_2$ (Figure 1a,b and Figure S1)[16, 18, 19]. As temperature increasing, greenish-yellow siloxene was converted to yellowish-brown SiO_x and brown nano-Si/*a*-SiO_2, finally become black color due to the surface-coated graphite (Figure 1c, Figure S2 and Figure S3). As shown in Figure S2, the d_{001} spacing of as-prepared siloxene (d = 0.56 nm) is found to be smaller than the corresponding quantity in Weiss siloxene (d = 0.63 nm)[20-22]. In this regard, and in order to confirm the formation of siloxene, FTIR spectrum shown in Figure 1d highlights the appearances of $(Si_2O)\equiv$Si-H, Si-Si and Si-OH stretching vibrations, in addition to Si-O-Si vibration, hence confirming that oxygen atoms are incorporated within Si_6 rings and some Si atoms are saturated by H and OH ligands[18, 20]. The assignments of the main absorption bands are listed in Table S1. Furthermore, the fragmentation of Si planes by insertion of oxygen is demonstrated also by the appearance of Raman peak at 495 cm^{-1} as well (dash dot line in Figure S4a)[19]. Herein, combining XRD, FTIR and Raman analysis (see the detail discussion in Figure S1-5), we demonstrate that the as-prepared siloxene exhibits Si (111) layers terminated above and below by H and OH ligands with Si_6 rings separated by oxygen atoms (Scheme S1 and annexed explanation)[16].

We have annealed the as-prepared siloxene under Ar atmosphere at 900 ºC, thus revealing the presence, in the XRD pattern of Figure S2, of both amorphous SiO_2 (a-SiO_2), defined by a broad bump $2\theta = 21.8^{o}$, and crystalline silicon at $2\theta = 28.4^{o}$[14]. The XRD diffraction patterns suggest that silicon suboxides are formed by a combination of a-SiO_2 and crystalline Si, which well agrees with amorphous SiO distinctively forming Si and SiO_2 when annealed at temperature higher than 800 ºC[23]. The low energy shift and broadening of Si-Si Raman peaks from ~515 to 502.7 cm^{-1} can instead be explained as a result of spatial confinement (Figure S4 and Figure S5)[24]. In particular, large silicon crystals are expected to display Raman shift similar to microcrystal or bulk Si (Figure S5)[24]. In our case, Raman analysis indicates that the size of Si nanodomains is certainly smaller than 30 nm, as shown by Figure 1e. Furthermore, the indistinctive Si signal in Figure 1f is interpreted in terms of wipe-out radius that is consistent with Si nanodomians[25, 26]. Similarly, the presence of a-SiO_2 was remarkably identified by ^{29}Si NMR.

In terms of the evolution from $CaSi_2$ to nano-Si/*a*-SiO_2@C, Figure 2 provides important insights. In particular, Figure 2a shows the lamellar structure of pristine $CaSi_2$ that was gradually delaminated into sheet-like siloxene in HCl aqueous solution (Figure 2b,c). After annealing, two dimensional feature could be preserved in nano-Si/*a*-SiO_2 composites (Figure S6). In addition, Figure 2d and Figure S7 displays sheet-like nano-Si/*a*-SiO_2@C coated with 5-10 nm amorphous carbon layer through CVD method. In the high-resolution TEM (HRTEM) image of Figure 2e, it is easy to identify abundant crystalline nanodomains with size less than 10 nm, well wrapped by amorphous matrix. The result is consistent with the calculated value ~15 nm from XRD pattern according Scherrer equation (Figure S2). In Figure 2f selected-area electronic diffraction (SAED) patterns disclose the *d* spacing of 0.310, 0.191 and 0.166 nm, corresponding to crystalline Si (111), (220) and (311), respectively. This result confirms the presence of crystalline silicon within nano-Si/*a*-SiO_2@C. Finally, electron energy loss spectroscopy (EELS) was applied to study the local electronic state of silicon as well as its distribution. Figures 2g,h show EELS images collected at different positions along a 100 nm line. As illustrated by Figure 2i, Si $L_{2,3}$ edges at ca. 100 and 107 eV are observed, characteristic of Si nanodomains and tetravalent silicon ions from the amorphous SiO_2 solid matrix, respectively. Importantly, all the Si $L_{2,3}$ spectra exhibit Si^0 and Si^{4+} characteristic peaks, owing to the encapsulation of Si nanodomains in the amorphous SiO_2 matrix. The fluctuating ratio of Si^0 to Si^{4+} peak intensity depends on the position being it related to the spatial distribution of Si nanodomians, as shown in Figure 2j. From these considerations, HRTEM, SAED and

EELS confirm the existance of Si crystal nanodomains that well agrees with the Raman results shown in Figure 1e. Furthermore, the presence of amorphous SiO_2 is verified by EELS Si $L_{2,3}$ edge and confirmed by ^{29}Si NMR.

Since, siloxene is relatively metastable confirmed by experimental and quantum chemical calculation[16, 27]. Furthermore, the existence of moisture and oxygen would result in OH substituting and Si-O-Si bond. Here, XPS was performed to evaluate the O/Si atomic ratio of siloxene based on the wide-range spectrum (Figure S8). The etching time 10 s corresponds to ca. 0.67 nm (more than d_{001} spacing of as-prepared siloxene). As shown in Figure 3a, the fresh as-prepared siloxene exhibits O/Si ratio 1.4, only 3~4 layers was oxidized after storing in air atmosphere for one week. To elucidate the stability and O/Si ratio in heat-aged siloxene, TG is a feasible method to calculate the O/Si ratio according the equation $SiO_x+O_2 \rightarrow SiO_2$. Two distinctive processes are shown in Figure S9, including the first step in the majority of dehydration (ΔW_1) and the second step associated with oxidation of SiO_x (ΔW_2). When the annealing temperature above 400 °C, ΔW_1 turning into stable indicates no more H_2O except adsorption water could be removed out off as-prepared siloxene, and the O/Si ratio decreases to ca. 1.1 (namely, $SiO_{1.1}$) and becomes constant (Figure 3b). After storing the 300 °C treated siloxene for 6 months, the surface and inner of silicon suboxide display $Si^{2.26+}$ and $Si^{2.24+}$, respectively, which are well consistent with *in-situ*/*ex-situ* TG results (Figure 3c,d, Figure S9). The similar results of the surface and inner could account for the stability of silicon suboxides.

The as-prepared siloxene is found to be an unsuitable anode for lithium ion batteries due to its poor electrochemical capacity, Coulombic efficiency and cycling stability (Figure S11). On the contrary, the sheet-like nano-Si/*a*-SiO_2@C composites exhibits excellent electrochemical performance. In particular, the nano-Si/*a*-SiO_2@C (C = 44.7 wt%, Figure S10) can deliver initial reversible capacity and Coulombic efficiency of 946.4 mAh g^{-1} and 72.5%, respectively, as shown in Figure 4a. The capacity increases to 982.5 mAh g^{-1} during the initial five charge/discharge cycles because of activation processes, followed by minor decay in the following cycles. This intriguing result becomes even more interesting when higher current densities rates are considered, as in Figure 4b,c and Figure S12c,d. In fact, while in previous works[11, 12, 14] silicon suboxides suffered from sluggish kinetics, our novel carbon coated sheet-like *a*-SiO_2 wrapped nano-Si electrode demonstrates excellent high rate capacity. The specific capacity of nano-Si/*a*-SiO_2@C composite anodes at 0.15, 0.3, 0.75 and 1.5 A g^{-1} are 950-980, ~930, ~800 and ~648 mA g^{-1}, respectively (Figure 4b and Figure S12b). The deposited carbon shows little contribution of capacity (Figure S13). With respect to MCMB, that is known to possess high electron conductivity and Li-ion diffusion coefficient, Figure S14 shows a delithiation capacity of just ~35 mAh g^{-1} at 7.5 A g^{-1}, corresponding only to 10.6 % of the specific capacity obtained at 0.15 A g^{-1} (~332 mAh g^{-1}). When the nano-Si/*a*-SiO_2@C composite is instead considered, a remarkable reversible capacity of ~360 mAh g^{-1} (38.0% with respect to 0.15 A g^{-1}) and good cycling performance (92% capacity retention after 300th cycles) are found at the noticeable rate of 7.5 A g^{-1}. This excellent result is summarized by the charge/discharge profiles in Figure S12c, displaying less than 6 min for one cycle at

7.5 A g^{-1}. With respect to previous works, the here introduced sheet-like nano-Si/*a*-SiO_2@C composite shows outstanding advantages especially in terms of rate capacity (Figure S12d), being capable indeed to meet fast charge/discharge requirements for exploiting the next generation of high-energy and high-power Li-ion batteries.

The choice of coating the composite with carbon is dictated by the need to improve its electronic conductivity and maintain the integrity of the sheet-architecture during cycling. In this regard, Figure 4d shows the reversible capacity decreasing from 1200 to 900 mAh g^{-1} with, however, the initial Coulombic efficiency (ICE) increasing from 62.0 to 75.5% upon amorphous carbon content change from 0 to 49.2 wt%. Because high ICE of deposited carbon (79.7%) would facilitate the ICE of nano-Si/*a*-SiO_2@C composite (Figure S13a). In terms of cycling performance, sheet-like nano-Si/*a*-SiO_2@C with 33.4 and 44.7 wt% carbon is illustrated in Figure 4e showing a capacity retention of 84% and 86% for 200 cycles under 0.75 A g^{-1}, respectively. As final and important note, we shall stress the role of early-cycles which are especially important because they account for most of Li-ion loss. Indeed, even for the best performing anodes the Coulombic efficiency takes many cycles to go above 99%. Remarkably, in Figure 4e we have demonstrated that our sheet-like nano-Si/a-SiO_2@C composite allows for the Coulombic efficiency to quickly rise up to 99.4 % in just five cycles.

An important characteristic of the sheet-like nano-Si/*a*-SiO_2@C material is its capability of maintaining structural integrity (Figure 5a,b) while forming irreversible lithium silicate (Figure 5c) after the first cycle at 0.15 A g^{-1}. In fact, it is well known that faster is the lithium ion insertion/extraction the more pronounced is the structural deterioration of the anode resulting in rapid capacity decay. In our case though the electrode surface displays only mild cracks while the thickness of the electrode increases of just 24% from 24.5 to 30.5 μm after 300 cycles at 7.5 A g^{-1}, as depicted in Figure 5d. This result is remarkably smaller than analogous reported quantities such as 42% (Si nanosheets electrode expansion after 200 cycles)[28], 51.3% (5 wt% graphene encapsulated Si electrode expansion after the first cycle)[29] and 38% (9 wt% Si included Si/Graphite electrode expansion after 50 cycles)[2]. This stable mechanical behavior is also manifested by an overall structural integrity after long cycling, such as the 300 cycles shown in Figure 4e.

To date, different electrochemical reaction mechanisms of SiO_2 during lithium ions insertion/extraction processes have been demonstrated[30, 31]. In particular, these works focus on the lithium silicate products $Li_2Si_2O_5$ or Li_4SiO_4[30-33]. In the sheet-like nano-Si/*a*-SiO_2@C system, the inactive Li_4SiO_4 material that is generated by *a*-SiO_2 after the first cycle is steadily maintained during the following 300th cycles as clearly shown by Figure 5c,e,f and also confirmed by the cathodic peak at 1.3 V in Figure S12a. In addition, the silicon generated via delithiation process is in the status of amorphous phase, it being consistent with the HRTEM results of Figure 5f .

Overall, the excellent rate capacity and cycling stability associated to nano-Si/*a*-SiO_2@C composite can be ascribed to the synergistic effect of Si nanodomains, amorphous SiO_2, surface carbon coating layer and sheet-like structure.

It has indeed been demonstrated that lithiation-induced fractures are strongly dependent on the size of Si[34]. Smaller Si size promises better durability. Herein, Si nanodomains (<10 nm) effectively delay cracks initiation and depress the particles pulverization which, combined with volume buffering effect from Li_4SiO_4 matrix, account for remarkable cycling performance. Furthermore, carbon coating layer enhances the electronic conductivity and keeps the integrity of sheet-like nano-Si/*a*-SiO_2. Besides, the 2D macrostructure configuration diminishes the Li-ion migration distance therefore improving the ionic conductivity. In summary, the proposed sheet-like nano-Si/*a*-SiO_2@C anode manifests limited volume expansion and structure deformation, fast electron and Li^+ diffusion mobility all together leading to remarkable cycle stability and rate performances.

Conclusion

We employ siloxene to fabricate sheet-like silicon suboxides nanocomposites ($SiO_{1.1}$), which exhibits Si nanodomains well-embedded into amorphous SiO_2 matrix. Our analyses verified that the as-prepared sheet-like siloxene is destroyed by oxygen atoms inserted into Si_6 rings, where Si dangling bonds are saturated with H and OH ligands. Owing to the synergistic effect of nanosized Si capable of suppressing the rising of fractures, inactive matrix of Li_4SiO_4 from *a*-SiO_2 as buffer layer to accommodate volume expansion, conductive carbon coating layer and 2D macrostructure, the sheet-like nano-Si/*a*-SiO_2@C anodes could exhibit an initial Coulombic efficiency as high as 72.5% and a capacity of 946 mAh g^{-1}, stable cycling performance and excellent rate capability. Approximately 360 mAh g^{-1} are delivered at 7.5 A g^{-1} in just less than 3 min of delithiation while 92% of capacity retention is achieved after 300 cycles. In short, our characterization has demonstrated that the sheet-like nano-Si/*a*-SiO_2@C material can indeed overcome the disadvantage of extreme volume expansion and poor rate capability, making it very attractive for the next generation of Li-ion batteries.

Acknowledgement

Financial supports from the National Natural Science Foundation of China (Grant No. 21371176), the National Key Research and Development Program of China (Grant No. 2016YFB0100100), Strategic Priority Research Program of Chinese Academy of Sciences (CAS, Grant No. XDA09010101) and Key Research Program of Chinese Academy of Sciences (Grant No. KGZD-EW-T08) are highly appreciated. We thank Dr. Guoxin Chen at NIMTE for his assistance in STEM-EELS characterization, and thank Dr. Xinmiao Liang and Prof. Jiwen Feng at WIPM for their assistances in solid-state NMR characterization.

Appendix A. Supplementary material

Supplementary data associated with this article can be found in the online version at……

References

[1] S. W. Lee, H. W. Lee, I. Ryu, W. D. Nix, H. J. Gao, Y. Cui, Nature Commun. 6 (2015) 7533-7539.

[2] M. Ko, S. Chae, J. Ma, N. Kim, H.-W. Lee, Y. Cui, J. Cho, Nature Energy 1 (2016) 16113-16120.

[3] X. H. Liu, L. Zhong, S. Huang, S. X. Mao, T. Zhu, J. Y. Huang, ACS Nano 6 (2012) 1522-1531.

[4] C.-F. Sun, H. Zhu, M. Okada, K. Gaskell, Y. Inoue, L. Hu, Y. Wang, Nano Lett. 15 (2015) 703-708.

[5] N. Liu, Z. D. Lu, J. Zhao, M. T. McDowell, H. W. Lee, W. T. Zhao, Y. Cui, Nature Nanotechnol. 9 (2014) 187-192.

[6] R. Yaokawa, T. Ohsuna, T. Morishita, Y. Hayasaka, M. J. S. Spencer, H. Nakano, Nature Commun. 7 (2016) 10657.

[7] J. Zhuang, X. Xu, G. Peleckis, W. Hao, S. X. Dou, Y. Du, Adv. Mater. (2017) DOI: 10.1002/adma.201606716.

[8] P. Paola De, O. Carlo, Q. Claudio, O. Bruno, I. Patrizia, S. Eric, A. Thierry, Q. Lucia, R. Claudia, V. Alessandro, M.-M. Maurizio, G. Amanda, P. Barbara, L. Guy Le, 2D Mater. 1 (2014) 021003.

[9] J. I. Lee, K. T. Lee, J. Cho, J. Kim, N. S. Choi, S. Park, Angew. Chem.-Int. Edit. 51 (2012) 2767-2771.

[10] C. M. Park, W. Choi, Y. Hwa, J. H. Kim, G. Jeong, H. J. Sohn, J. Mater. Chem. 20 (2010) 4854-4860.

[11] S. S. Suh, W. Y. Yoon, D. H. Kim, S. U. Kwon, J. H. Kim, Y. U. Kim, C. U. Jeong, Y. Y. Chan, S. H. Kang, J. K. Lee, Electrochim. Acta 148 (2014) 111-117.

[12] E. Park, H. Yoo, J. Lee, M. S. Park, Y. J. Kim, H. Kim, ACS Nano 9 (2015) 7690-7696.

[13] M. K. Kim, B. Y. Jang, J. S. Lee, J. S. Kim, S. Nahm, J. Power Sources 244 (2013) 115-121.

[14] M. S. Park, E. Park, J. Lee, G. Jeong, K. J. Kim, J. H. Kim, Y. J. Kim, H. Kim, ACS Appl. Mater. Inter. 6 (2014) 9608-9613.

[15] J. R. Dahn, B. M. Way, E. Fuller, J. S. Tse, Phys. Rev. B 48 (1993) 17872-17877.

[16] H. Nakano, M. Ishii, H. Nakamura, Chem. Commun. (2005) 2945-2947.

[17] S. C. Jung, H.-J. Kim, J.-H. Kim, Y.-K. Han, J. Phys. Chem. C 120 (2016) 886-892.

[18] N. Delpuech, D. Mazouzi, N. Dupré, P. Moreau, M. Cerbelaud, J. S. Bridel, J. C. Badot, E. De Vito, D. Guyomard, B. Lestriez, B. Humbert, J. Phys. Chem. C 118 (2014) 17318-17331.

[19] H. D. Fuchs, M. Stutzmann, M. S. Brandt, M. Rosenbauer, J. Weber, A. Breitschwerdt, P. Deak, M.

Cardona, Phys. Rev. B 48 (1993) 8172-8183.

[20] S. Yamanaka, H. Matsu, M. Ishikawa, Mater. Res. Bull. 31 (1996) 307-316.

[21] U. Dettlaff-Weglikowska, W. Honle, A. MolassiotiDohms, S. Finkbeiner, J. Weber, Phys. Rev. B 56 (1997) 13132-13140.

[22] H. Nakano, M. Nakano, K. Nakanishi, D. Tanaka, Y. Sugiyama, T. Ikuno, H. Okamoto, T. Ohta, J. Am. Chem. Soc. 134 (2012) 5452-5455.

[23] A. Hirata, S. Kohara, T. Asada, M. Arao, C. Yogi, H. Imai, Y. Tan, T. Fujita, M. Chen, Nature Commun. 7 (2016) 11591-11597.

[24] H. D. Fuchs, M. Stutzmann, M. S. Brandt, M. Rosenbauer, J. Weber, M. Cardona, Phys. Scripta T45 (1992) 309-313.

[25] A. Hohl, T. Wieder, P. A. van Aken, T. E. Weirich, G. Denninger, M. Vidal, S. Oswald, C. Deneke, J. Mayer, H. Fuess, J. Non-Cryst. Solids 320 (2003) 255-280.

[26] J.-H. Kim, C.-M. Park, H. Kim, Y.-J. Kim, H.-J. Sohn, J. Electroanal. Chem. 661 (2011) 245-249.

[27] P. Deak, M. Rosenbauer, M. Stutzmann, J. Weber, M. S. Brandt, Phys. Rev. Lett. 69 (1992) 2531-2534.

[28] J. Ryu, D. Hong, S. Choi, S. Park, ACS Nano 10 (2016) 2843-2851.

[29] I. H. Son, J. Hwan Park, S. Kwon, S. Park, M. H. Rümmeli, A. Bachmatiuk, H. J. Song, J. Ku, J. W. Choi, J.-m. Choi, S.-G. Doo, H. Chang, Nature Commun. 6 (2015) 7393-7400.

[30] W. S. Chang, C. M. Park, J. H. Kim, Y. U. Kim, G. Jeong, H. J. Sohn, Energy Environ. Sci. 5 (2012) 6895-6899.

[31] N. Yan, F. Wang, H. Zhong, Y. Li, Y. Wang, L. Hu, Q. W. Chen, Sci. Rep. 3 (2013) 1568-1573.

[32] B.-C. Yu, Y. Hwa, C.-M. Park, H.-J. Sohn, J. Mater. Chem. A 1 (2013) 4820-4825.

[33] M. Yamada, A. Inaba, A. Ueda, K. Matsumoto, T. Iwasaki, T. Ohzuku, J. Electrochem. Soc. 159 (2012) A1630-A1635.

[34] L. L. Luo, P. Zhao, H. Yang, B. R. Liu, J. G. Zhang, Y. Cui, G. H. Yu, S. L. Zhang, C. M. Wang, Nano Lett. 15 (2015) 7016-7022.

Rusheng Fu received his B.S. degree in Materials Science and Engineering from Nanchang University in 2009, and his M.Eng. degree in College of Materials from Xiamen University (China), in 2012. He is now a Ph.D. candidate under the supervision of Prof. Zhaoping Liu in Ningbo Institute of Materials Technology and Engineering, Chinese Academy of Sciences. Currently, his research interests mainly focus on the development of high specific capacity anode materials for lithium ion batteries.

Keli Zhang received her B.S. degree in Safety Engineering from Anhui University of Science and Technology in 2010. She is now a M.Eng. candidate in University of Science and Technology of China. And she is Joint-Supervision student under the supervision of Prof. Zhaoping Liu in Ningbo Institute of Materials Technology and Engineering, Chinese Academy of Sciences. Her current research interests mainly focus on the applications of silicon/carbon composites anode materials for lithium ion batteries.

Remo Proietti Zaccaria is Professor at the Cixi Institute of Biomedical Engineering, Ningbo Institute of Materials Technology and Engineering, Chinese Academy of Sciences and group leader of the Multiphysics laboratory at the Italian Institute of Technology. His work mainly aims in modelling and experimentally validate complex systems at the micro/nano-scale with strong emphasis on the final device. In particular, his research themes focus on the integration of different physics (i.e. interdisciplinary) such as photonics, heat diffusion, electric charge/mass diffusion and mechanical-deformation towards the development of innovative devices for energy manipulation (harvesting and storage).

Heran Huang received his B.Eng. in 2015 from China University of Petroleum, Beijing and obtained his M.S. degree in 2016 from University of Nottingham, U.K. He is now serving as a research assistant in Advanced Lithium-ion Battery Engineering Lab, Ningbo Institute of Materials Technology & Engineering, Chinese Academy of Sciences. His research interests focus on anode materials for lithium ion supercapacitors.

Yonggao Xia received his Ph.D. in Energy and Materials Science from Saga University, Japan, in 2008, after which he worked as a researcher at New Products Development Division in Kanto Denka Kogyo Co., Ltd., Japan. He is currently the professor in Advanced Lithium-ion Battery Engineering Lab, Ningbo Institute of Materials Technology & Engineering, Chinese Academy of Sciences. His research interests focus on advanced materials and technologies for lithium-ion batteries.

Zhaoping Liu received his Ph.D. in inorganic chemistry from University of Science & Technology of China in 2004. Then he worked as a postdoctoral researcher in National Institute for Material Science, Japan, and State University of New York at Binghamton, between 2004 and 2008. Since October 2008, he has worked in Ningbo Institute of Materials Technology and Engineering, Chinese Academy of Sciences. He currently is the Director of Advanced Li-ion Battery Engineering Laboratory and Key Laboratory of Graphene Technologies and Applications of Zhejiang Province. His main research interests include Li-ion batteries and graphene.

Figure Captions:

Figure 1. Structural design and characterization of the as-prepared siloxene and nano-Si/*a*-SiO_2@C. (a) Illustrations of the transformation evolution from layered $CaSi_2$ to siloxene. (b) Structure of as-prepared siloxene. (c) Schematic illustration of nano-Si/*a*-SiO_2@C composites. (d) FTIR spectrum for the as-prepared siloxene (blue line) and nano-Si/*a*-SiO_2@C (red line). e) Raman characterization is applied to distinguish among different Si particle sizes. Full width at half maximum (Γ) of the Raman peak vs. frequency shift ($\Delta\omega$) starting from the position of microcrystalline silicon. Microcrystal silicon (μ-Si, 75 μm), 100 nm and 30 nm Si particles are shown for comparison. f, ^{29}Si MAS NMR spectrum reveals Si nanodomains (-60~-90 ppm) and amorphous silicon dioxide (-110 ppm).

Figure 2. Evolution processes from layered $CaSi_2$ to nano-Si/*a*-SiO_2@C. (a) SEM image of $CaSi_2$ with pronounced lamellar structure. (b, c) TEM images showing the partial delaminated (b) and in-depth delaminated (c) siloxene materials. (d) TEM image of sheet-like nano-Si/*a*-SiO_2@C. The inset shows the amorphous carbon coating layer marked with white dash line. (e) HRTEM image showing nano-Si lattice fringes as highlighted by white dotted lines separated by amorphous phase (*a*-SiO_2). (f) SAED patterns confirm the presence of crystalline silicon phase in nano-Si/*a*-SiO_2@C. (g) STEM image of nano-Si/*a*-SiO_2@C. (h) STEM-EELS spectra from the black line (0-100 nm) in the STEM image (g) showing Si $L_{2,3}$ edge. The dispersion is 0.1 eV/channel. The scan step is 0.5 nm. (i) EELS spectra profiles of Si $L_{2,3}$ edge marked with the same sequence as in (h). Each spectrum was averaged vertically with 10 individual spectra to improve the signal to noise ratio. (j) Relative ratio of intensity I(Si)/I(Si^{4+}) as a function of position is calculated based on the integrated EELS peak intensity in (h).

Figure 3. Storage stability and O/Si atomic ratio of as-prepared siloxene and annealed samples. (a) Storage stability of as-prepared siloxene before and after storing in air for one week. (b) O/Si atomic ratio at various annealing temperature. (c, d) The

deconvolution of Si 2p in 300 °C aged siloxene undergoing 6 months storage in air without (c) and with (d) 1 min etching, respectively.

Figure 4. Electrochemical performance of nano-Si/*a*-SiO_2@C. (a) Galvanostatic charge/discharge profiles of nano-Si/*a*-SiO_2@C electrode upon different cycles at 0.15 A g^{-1}. (b) Rate performance at different current densities for nano-Si/*a*-SiO_2@C. (c) Cycling performance at various current densities for nano-Si/*a*-SiO_2@C measured at 1.5, 3.0 and 7.5 A g^{-1}, respectively. The first three activating cycles are ran at 0.3 A g^{-1} while the following 300 cycles are subjected to higher rates. (d) Reversible capacity and initial Coulombic efficiency of nano-Si/*a*-SiO_2@C with various carbon contents: 0, 33.4, 44.7 and 49.2 wt%. (e) Comparison of the nano-Si/*a*-SiO_2@C cycling performance for 33.4 and 44.7 wt% carbon content at 0.75 A g^{-1} after the first two activating cycles are ran at 0.15 A g^{-1}. All the specific capacities are reported based on the active materials (nano-Si/*a*-SiO_2@C). In a-c the carbon content is equal to 44.7 wt%.

Figure 5. Characterization of nano-Si/*a*-SiO_2@C before and after charge/discharge. (a, b) HRTEM images of sheet-like nano-Si/*a*-SiO_2@C after the first cycle. (c) SAED spots corresponding to the orange circle in (b) indicating that the crystal lithium silicate Li_4SiO_4 was formed during the first lithiation process. (d) Electrode surface morphologies before cycling test (up left) and after 300 cycles (up right) at 7.5 A g^{-1}. Cross-sectional morphologies before cycling test (down left) and after 300 cycles (down right) at 7.5 A g^{-1}. (e) TEM image of nano-Si/*a*-SiO_2@C after 300 cycles. The SAED spots (inset) are from Li_4SiO_4 (-210) planes. Scale bar, 5 1/nm. (f) HRTEM image and faster Fourier transformation spots (inset) showing remarkable lattice fringes of Li_4SiO_4 and amorphous phase (mostly Si), respectively. The image was taken after 300 cycles.

Research highlights

- Sheet-like silicon suboxides are first prepared by delaminated siloxene which derives topotactic transformation of layered $CaSi_2$.
- Silicon suboxides exhibit Si nanodomains confined in amorphous SiO_2.
- The delicate designed carbon coated silicon suboxides anodes deliver superior cycling performance and rate capability.

Figure 1

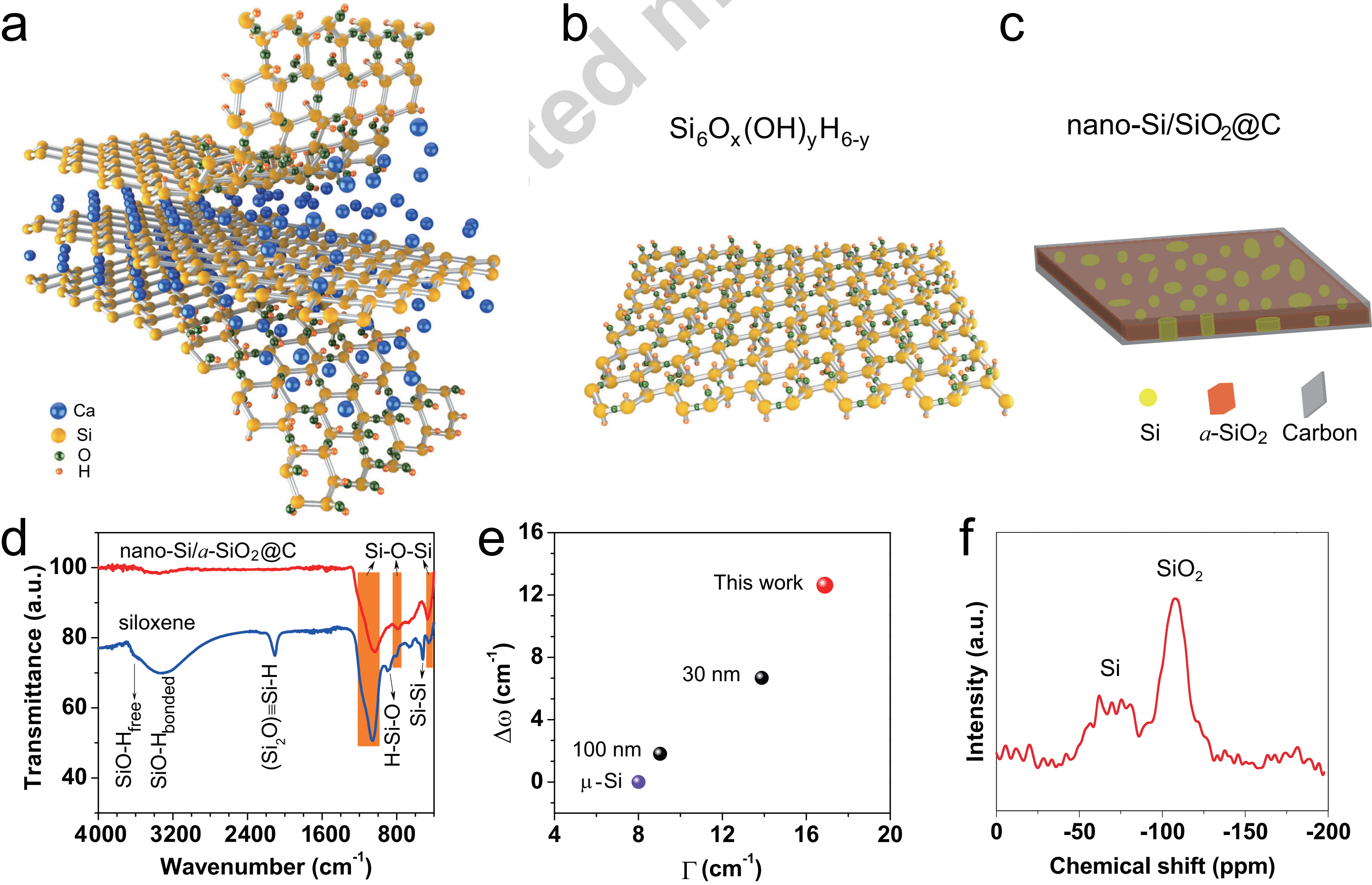
a
Ca
Si
O
H
b
Si6Ox(OH)yH6-y
c
nano-Si/SiO2@C
Si
a-SiO2
Carbon
d
nano-Si/a-SiO2@C
siloxene
Si-O-Si
SiO-Hfree
SiO-Hbonded
(Si2O)≡Si-H
H-Si-O
Si-Si
Transmittance (a.u.)
100
80
60
40
4000
3200
2400
1600
800
Wavenumber (cm-1)
e
This work
30 nm
100 nm
μ-Si
Δω (cm-1)
16
12
8
4
0
4
8
12
16
20
Γ (cm-1)
f
SiO2
Si
Intensity (a.u.)
0
-50
-100
-150
-200
Chemical shift (ppm)

Figure 2

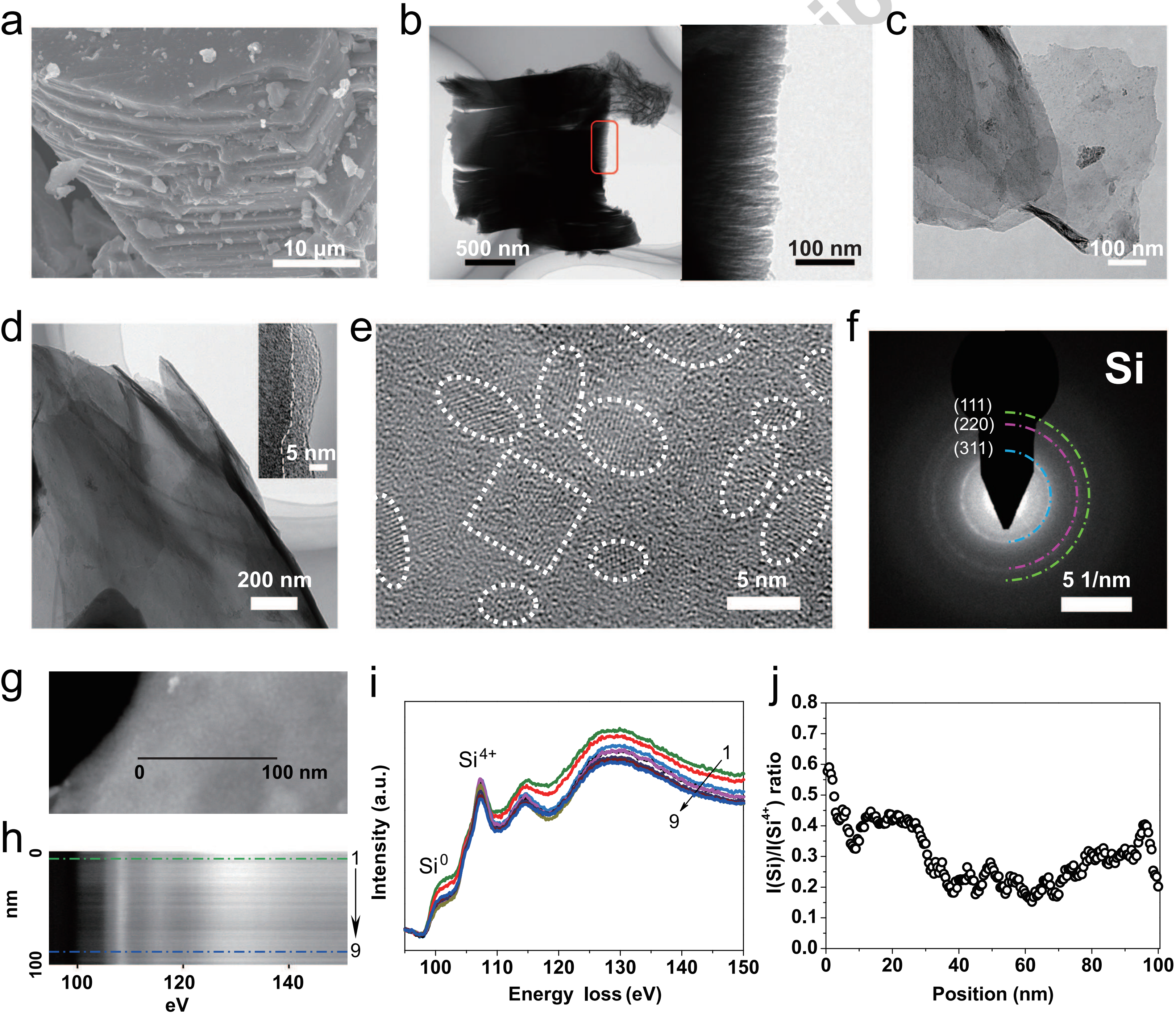
a
10 µm
b
500 nm
100 nm
c
100 nm
d
5 nm
200 nm
e
5 nm
f
Si
(111)
(220)
(311)
5 1/nm
g
0
100 nm
h
0
nm
100
1
9
100
120
140
eV
i
Si^{4+}
Si^{0}
1
9
Intensity (a.u.)
100
110
120
130
140
150
Energy loss (eV)
j
0.8
0.7
0.6
0.5
0.4
0.3
0.2
0.1
0.0
I(Si)/I(Si^{4+}) ratio
0
20
40
60
80
100
Position (nm)

Figure 3

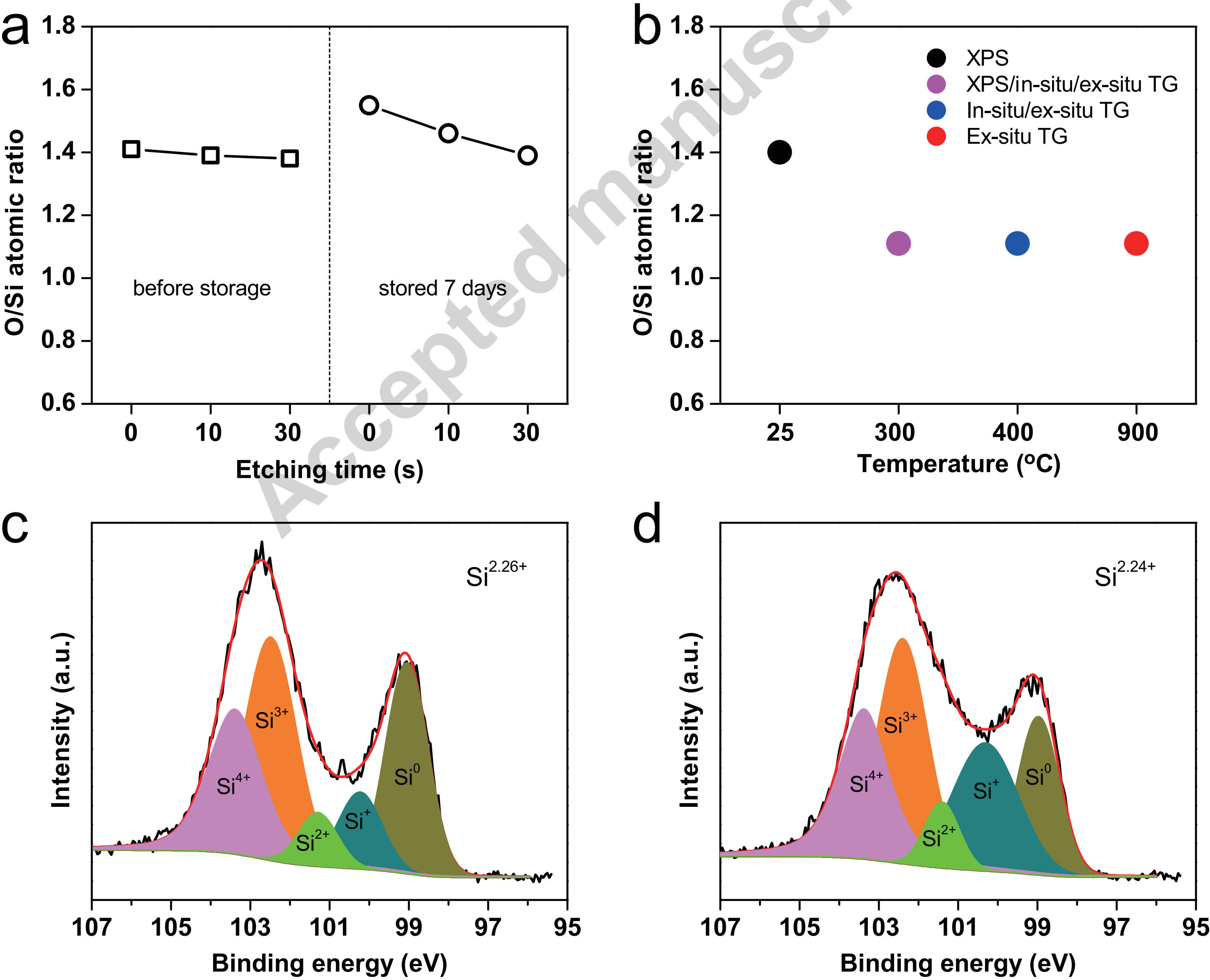
a
O/Si atomic ratio
1.8
1.6
1.4
1.2
1.0
0.8
0.6
before storage
stored 7 days
0
10
30
0
10
30
Etching time (s)
b
XPS
XPS/in-situ/ex-situ TG
In-situ/ex-situ TG
Ex-situ TG
25
300
400
900
Temperature (°C)
c
Intensity (a.u.)
$Si^{2.26+}$
Si^{4+}
Si^{3+}
Si^{2+}
Si^{+}
Si^{0}
107
105
103
101
99
97
95
Binding energy (eV)
d
$Si^{2.24+}$
Binding energy (eV)

Figure 4

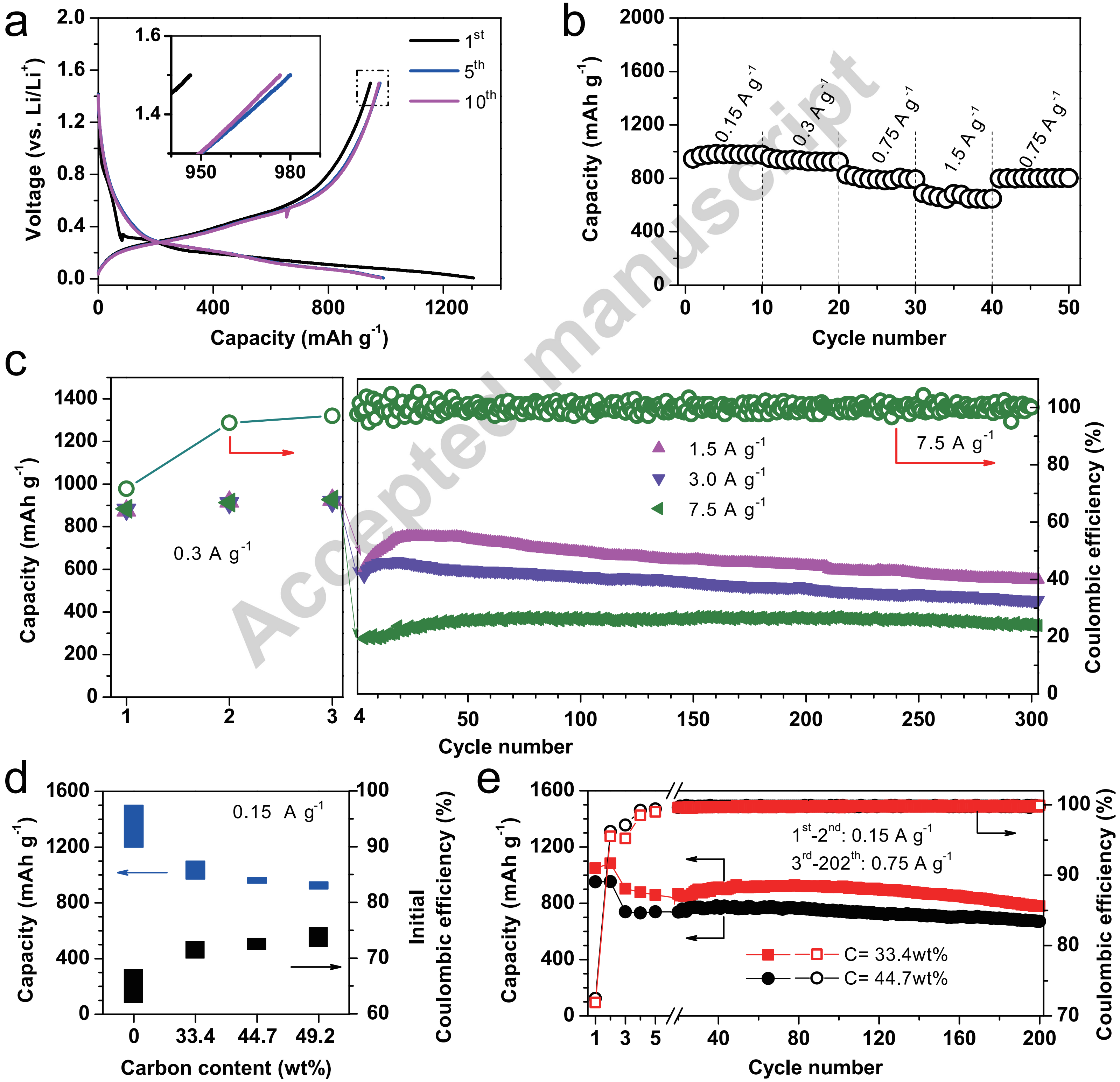
a
Voltage (vs. Li/Li$^+$)
2.0
1.6
1.2
0.8
0.4
0.0
0
400
800
1200
Capacity (mAh g^{-1})
1.6
1.4
950
980
1st
5th
10th
b
Capacity (mAh g^{-1})
2000
1600
1200
800
400
0
0.15 A g^{-1}
0.3 A g^{-1}
0.75 A g^{-1}
1.5 A g^{-1}
0.75 A g^{-1}
0
10
20
30
40
50
Cycle number
c
Capacity (mAh g^{-1})
1400
1200
1000
800
600
400
200
0
0.3 A g^{-1}
1
2
3
4
50
100
150
200
250
300
Cycle number
1.5 A g^{-1}
3.0 A g^{-1}
7.5 A g^{-1}
7.5 A g^{-1}
Coulombic efficiency (%)
100
80
60
40
20
0
d
Capacity (mAh g^{-1})
1600
1200
800
400
0
0.15 A g^{-1}
0
33.4
44.7
49.2
Carbon content (wt%)
100
90
80
70
60
Initial Coulombic efficiency (%)
e
Capacity (mAh g^{-1})
1600
1200
800
400
0
1
3
5
40
80
120
160
200
Cycle number
1st-2nd: 0.15 A g^{-1}
3rd-202th: 0.75 A g^{-1}
C= 33.4wt%
C= 44.7wt%
Coulombic efficiency (%)
100
90
80
70

Figure 5

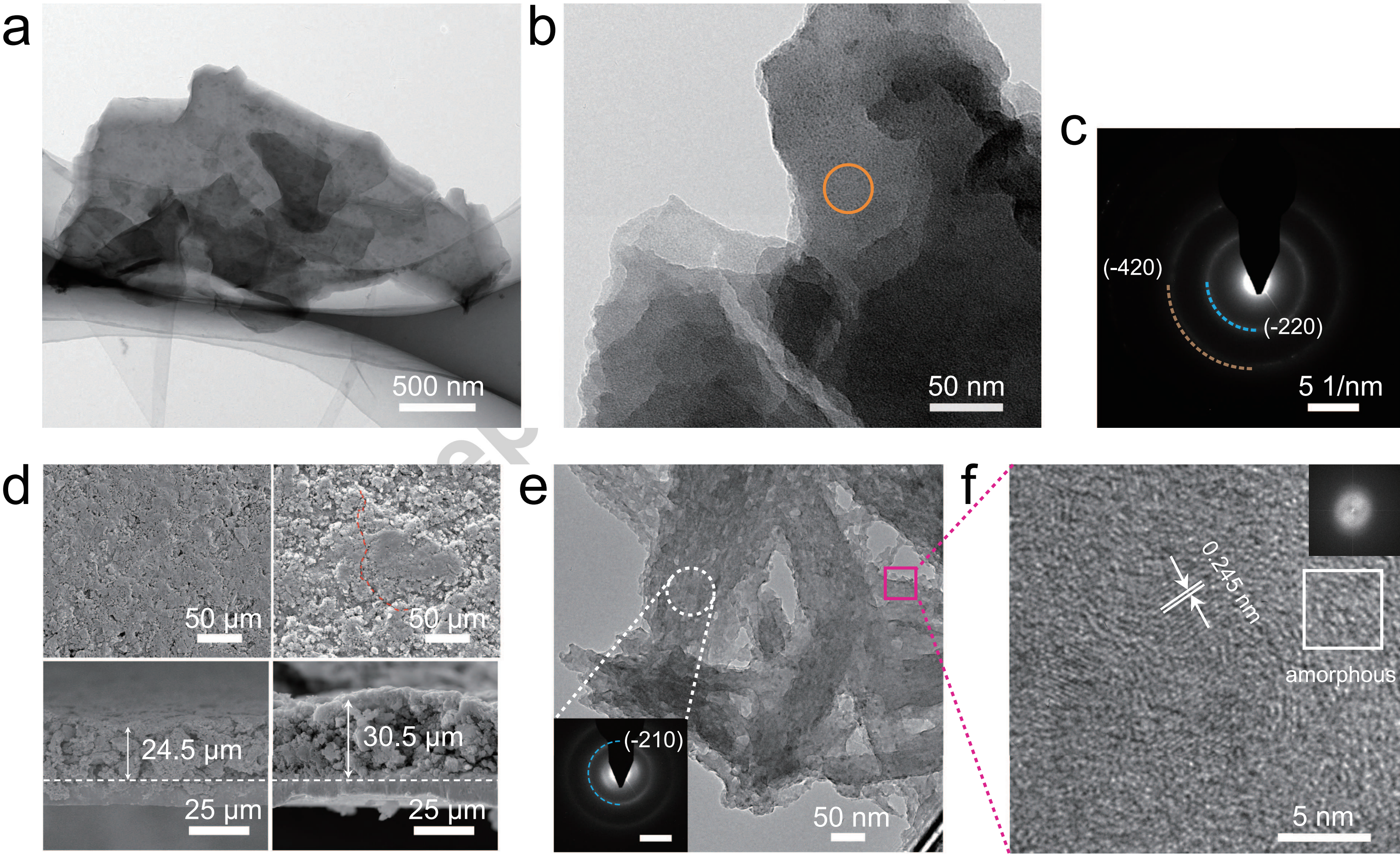
a
500 nm
b
50 nm
c
(-420)
(-220)
5 1/nm
d
50 μm
50 μm
24.5 μm
30.5 μm
25 μm
25 μm
e
(-210)
50 nm
f
0.245 nm
amorphous
5 nm